Heterogeneous Colloidal Particles Immersed in a Liquid Crystal

Setarehalsadat Changizrezaei*
Department of Physics and Astronomy, The University of Western Ontario, London, Ontario N6A 5B8, Canada.

Colin Denniston†
Department of Applied Mathematics, The University of Western Ontario, London, Ontario N6A 5B8, Canada. and Department of Physics and Astronomy, The University of Western Ontario, London, Ontario N6A 5B8, Canada.

(Dated: July 9, 2017)

In this paper, we explore anisotropic interactions between particles with heterogeneous boundary conditions inside both nematic and cholesteric liquid crystals. The results show that when particles are put at different distances and angles with respect to each other, new types of defect structures are produced, depending on the relative distances and directions. In a cholesteric liquid crystal, the value of the pitch affects the defect structures and induced forces. Moreover, it was observed that it is energetically favorable for the particles to remain in a plane parallel to the far-field director in a nematic liquid crystal, while for particles immersed in a cholesteric there are multiple energy minima not all located in the same plane.

PACS numbers: 61.30.Jf 47.57.J

I. INTRODUCTION

Over the past few decades, self-assembly of colloidal particles in a fluid has been suggested as an efficient method to manufacture photonic crystals [1–5]. Photonic crystals are created from a structure with a periodic dielectric constant. They can be used to confine and control light propagation in an analogous manner to electron propagation in semiconductors [5, 6], if they possess a photonic band gap. In an isotropic fluid, colloidal particles typically form closed-packed crystals such as fcc and hcp, which do not show a "complete band gap". The anisotropic properties of liquid crystals make them an appropriate medium for colloidal particles to generate anisotropic interactions and potentially form non-closed packed structures, such as a diamond lattice, that can exhibit a complete band gap.

If colloidal particles are present in a liquid crystal (LC), due to the preferred anchoring of molecules on the colloid surface, the director becomes distorted from its uniform alignment. As a result, topological defects are generated around the particles [7]. The preferred anchoring of LC molecules on the surface of particles is most typically parallel (planar anchoring), or perpendicular (normal or homeotropic anchoring) [8]. For a spherical colloidal particle with *planar* anchoring in a nematic LC a pair of defects are created at the poles of particles, called boojums [7]. There are three types of boojum cores: single, split, and double core [9]. The single core is axially symmetric and point-like with index +1. It is stable for small particles with relatively weak anchoring, and at higher temperatures. On the other hand, at low temperatures, strong anchoring, and for large colloidal particles, the cores split into pairs of $+\frac{1}{2}$ point defects which are connected with a disclination line of the same strength. The double core boojum refers to an intermediate structure in which the disclination line is not completely developed. In the case of *normal* anchoring, two possible defect structures may be produced in a nematic. One possible structure is a -1 point defect, called a hyperbolic hedgehog [10], located near the surface of the colloidal. Another possibility is a disinclination ring surrounding the particle referred to as a Saturn-ring defect [11–13]. The particle radius and anchoring strength dictates which structure is generated. Typically the Saturn ring is a stable structure for small particles, while the hedgehog point is produced for large particles [8].

These defect structures produce long-range anisotropic interactions between the particles, many of which have been mapped out experimentally [44]. When the particles are far from each other, the interaction energy between them is dictated by the long range orientational field. For instance, particles with boojums in planar anchoring, or particles with Saturn rings in normal anchoring, induce elastic "quadrupolar"[7] distortions, and corresponding interactions. Colloidal particles with hyperbolic hedgehog defects in a nematic liquid crystal, there is a different kind of interaction. In the far-field approximation, the particle-defect pair has a "dipole"[7] symmetry and corresponding effective interactions.

When the particles get close to each other, their interactions can deviate from the expectations of the far-field approximation due to local distortions around the defect structures [14, 15]. For example, experiments observed that as two particles with planar anchoring approach each other, they attract each other when the line between their centers is oriented at $\theta = 30$ from the far-filed director $\hat{\mathbf{n}}$ and there is a repulsion at $75^\circ < \theta < 90^\circ$, which is different from the far-field interaction [15]. These sorts

*Electronic address: schangiz@uwo.ca
†Electronic address: cdennist@uwo.ca

of interactions, combined with optical manipulation result in a broad variety of one and two-dimensional nematic colloidal crystals[45], including linear chains[18], "kinked" chains [19], which can be combined to form close-packed two dimensional crystals [43]. At high concentrations it has also been demonstrated that a three-dimensional defect glass state can be formed where the mechanical strength is a result of a percolated network of defect lines entangled with the clustered colloids[36].

One of the few non-close packed ordered nematic colloid systems was found by looking at a binary mixture of particles with homeotropic and planar anchoring[38]. The experiments showed that such a binary system of colloids in a nematic LC can be used to build a 2D square colloid crystal. We will perform simulations related to this case here before looking at similar binary pairs in cholesterics.

When a spherical colloid is placed in a cholesteric LC, the defect lines become twisted around the particles. These structures can be controlled by the value of the pitch in cholesteric. In both cases of planar and normal anchoring, the defect lines wind around the particles as the pitch value decreases [16]. The interactions produced by colloidal particles with planar anchoring, was investigated by Mackay and Denniston in [17]. In this case, the defects on the adjacent particles connect to each other when they are close to each other, and a defect bonded particle chain is generated. The ratio of the pitch length of the cholesteric to the particle size turns out to be an important factor in the colloidal self-organization. For example, two-dimensional planar structures are found to preferentially form over chains for shorter pitches [46] and this effect is evident even in examining the interaction energies of pairs of such particles [17]. The dynamics of pairs of colloids with planar anchoring in a cholesteric is also very unusual. When pulled through the cholesterical by a constant force along the helical axis, the dimer rotate continuously or with phase-slip events [40].

Interestingly, the attractive forces between two spherical colloids with strong normal anchoring in a cholesteric are oscillatory functions of particle separation and can be controlled through the chirality of the medium. The strongest interaction between the particles occurs at the pitch value equal to particle diameter. As the chirality increases, the strength of the interaction decreases, and the pair potential is screened [39]. It is also possible to find a locally stable diamond colloidal crystal structure for colloids with normal anchoring in a cholesteric by adjusting the ratio of pitch to particle size [20], although how to get the colloids into this state is still unclear. However, a wide variety of particle-induced defect structures have been found and optical guiding by laser tweezers has been used to produce a complex variety of 2D and 3D assembly of particles so far [41].

A variety of structures can also be found in more exotic liquid crystals-colloid mixtures[42]. In colloidal-blue phase composites, in which the director twists in more than one direction, the colloidal particles can be attracted to the 3D disclination network produced by blue phase LC so that the elastic stresses are decreased at the disclination cores and stable close-packed three dimensional crystals can be formed [35]. By adjusting the anchoring strength, one can manipulate the tendency for colloids to cluster and form disclination networks leading to a variety of interesting structures[37].

Many semiconductors, such as GaAs or InSb, are composed of two different elements in a zinc blende lattice. In the search for materials that might exhibit a photonic band gap this provides motivation to investigate compound colloidal structures. In this work, we analyze induced interactions between particles with different sorts of surface anchoring, planar and normal, when immersed in both nematic and cholesteric liquid crystals. The paper is organized as follows: In section II, we describe the Landau-de Gennes free energy approach and Beris-Edwards formulation to model the evolution of the liquid crystal tensor order parameter. In section III, we examine defect structures of each of the individual particles with planar and normal anchoring separately, and explore interactions between these two static particles as well as their defect structures inside both nematic and cholesteric LC with different pitch values, relative to the size of the particles. Our findings for static particles are then confirmed by further investigation of freely moving particles.

II. MODELING

Using Landau-de Gennes theory to model the LC, a tensor order parameter $\boldsymbol{Q}$ is introduced as a mathematical tool to describe the LC orientation [21]. This tensor is defined as a coarse-grained average of each molecule orientations, $\hat{m}$:

$$Q_{ij} = \langle \frac{3}{2}\hat{m_i}\hat{m_j} - \frac{1}{2}\delta_{ij} \rangle \,. \tag{1}$$

Q is a symmetric traceless 3×3 matrix, with largest eigenvalue $\frac{2}{3}q$, $0 < q < 1$, indicating the magnitude of order along the director $\hat{n}$, corresponding to the principal eigenvector. In this case, the total energy of the system is described as:

$$F = \int dV \left\{ F_{bulk} + F_{elastic} \right\} + \int F_{surface}\, dS \,. \tag{2}$$

Here, F_{bulk} is the bulk free energy of the system which can be described using a Landau expansion:

$$F_{bulk} = \frac{A_0}{2}(1-\frac{\gamma}{3})Q_{\alpha\beta}^2 - \frac{A_0\gamma}{3}Q_{\alpha\beta}Q_{\beta\gamma}Q_{\gamma\alpha} + \frac{A_0\gamma}{4}\left(Q_{\alpha\beta}^2\right)^2 \,, \tag{3}$$

where A_0 is a constant, and γ distinguishes between liquid crystalline from the isotropic phase. The isotropic fluid is the stable phase when $\gamma < 2.7$. Here, γ is set to 3.1 in order to be in the liquid crystalline phase.

The elastic distortions are represented in $F_{elastic}$ as:

$$F_{elastic} = \frac{L_1}{2}(\partial_\alpha Q_{\beta\gamma})^2 + \frac{L_2}{2}(\partial_\alpha Q_{\alpha\gamma})(\partial_\beta Q_{\beta\gamma}) \frac{4\pi L_1}{P}\epsilon_{\alpha\beta\gamma}Q_{\alpha\nu}(\partial_\beta Q_{\gamma\nu}), \quad (4)$$

where the elastic constants, L_1 and L_2, can be mapped to the Frank elastic constants, K_1, K_2, K_3 [22]. For nematic simulations, we used the one elastic constant approximation, in which $L_2 = 0$, while to have a realistic stable cholesteric LC we chose K_2 smaller than K_1 and K_3 and $K_1 = K_2$. The presence of the last term is essential to model a cholesteric LC with a helical pitch, P, in the director.

In addition to the bulk and elastic energy, the interaction of LC molecules with external surfaces and colloidal particles must be considered as well, which is represented by $F_{surface}$. This is characterized by the preferred orientation of the LC, applied by the surface boundary conditions, and the anchoring strength α_s. In our work, we used both planar and normal alignment of the LC molecules on different surfaces, which can be imposed by the following expressions:

$$F_{surface} = \frac{\alpha_s}{2}(Q_{ij} - Q^0_{ij})^2 \rightarrow Normal\ anchoring, \quad (5)$$

$$F_{surface} = \frac{\alpha_s}{2}(\tilde{Q_{ij}} - \tilde{Q_{ij}}^{\perp})^2 \rightarrow Planar\ anchoring, \quad (6)$$

Here, $\boldsymbol{Q}^0$ is chosen as $Q^0_{ij} = q^0(\hat{n_i}^0\hat{n_j}^0 - \frac{1}{3}\delta_{ij})$, where $\hat{n}^0$ is the normal to the surface of particle, and q^0 is the equilibrium bulk value of q. $\tilde{\boldsymbol{Q}}$ in Eq. (6) can be written as $\tilde{Q_{ij}} = Q_{ij} + \frac{1}{3}q^0\delta_{ij}$ and $\tilde{Q_{ij}}^{\perp} = (\delta_{ik} - \hat{n_i}^0\hat{n_k}^0)\tilde{Q_{kl}}(\delta_{lj} - \hat{n_l}^0\hat{n_j}^0)$ is the projection of $\tilde{Q_{ij}}$ onto the tangent plane of the surface [23]. On the system's walls, there is also a planar anchoring. However, since the molecules are only oriented along one specific direction, $\hat{y}$ or $\hat{x}$, on the walls, we used Eq. (5) to set $\hat{n}$ along this specific direction.

A. Liquid Crystal Hydrodynamics

The evolution of the order parameter is tracked using the Beris-Edwards formulation [22]:

$$(\partial_t + \boldsymbol{u}\cdot\nabla)\boldsymbol{Q} - \boldsymbol{S}(\boldsymbol{W},\boldsymbol{Q}) = \Gamma\boldsymbol{H}, \quad (7)$$

with

$$\boldsymbol{S}(\boldsymbol{W},\boldsymbol{Q}) = (\xi\boldsymbol{D} + \Omega)(\boldsymbol{Q} + \boldsymbol{I}/3) + (\boldsymbol{Q} + \boldsymbol{I}/3)(\xi\boldsymbol{D} - \boldsymbol{\Omega}) - 2\xi(\boldsymbol{Q} + \boldsymbol{I}/3)Tr(\boldsymbol{QW}), \quad (8)$$

where $\boldsymbol{D} = (\boldsymbol{W} + \boldsymbol{W}^T)/2$ and $\boldsymbol{\Omega} = (\boldsymbol{W} - \boldsymbol{W}^T)/2$ correspond to the symmetric and antisymmetric parts of the velocity gradient tensor $W_{\alpha\beta} = \partial_\beta u_\alpha$, and the effective aspect ratio of liquid crystal molecules is described by ξ, and Γ is the collective rotational diffusion constant. The right hand side of Eq. (7) drives the system towards the minimum of the free energy, and H is related to the functional derivative of the free energy:

$$\boldsymbol{H} = -\frac{\delta F}{\delta Q} + \left(\frac{\boldsymbol{I}}{3}\right)\frac{\delta F}{\delta Q}. \quad (9)$$

As the liquid crystal is a fluid, it should satisfy the continuity and Navier-Stokes equations. However, the stress tensor in these equations contains the additional complexities of the liquid crystal which has both symmetric

$$\sigma_{\alpha\beta} = -P_0\delta_{\alpha\beta} - \xi H_{\alpha\gamma}(Q_{\gamma\beta} + \frac{1}{3}\delta_{\alpha\beta}) - \xi(Q_{\alpha\gamma} + \frac{1}{3}\delta_{\alpha\gamma})H_{\alpha\beta} + 2\xi(Q_{\alpha\beta} + \frac{1}{3}\delta_{\alpha\beta})Q_{\gamma\epsilon}H_{\gamma}\epsilon - \partial_\beta Q_{\gamma\nu}(\frac{\delta F}{\delta\partial_\alpha Q_{\gamma\nu}}), \quad (10)$$

and antisymmetric

$$\tau_{\alpha\beta} = Q_{\alpha\gamma}H_{\gamma\beta} - H_{\alpha\gamma}Q_{\alpha\beta}, \quad (11)$$

components.

In our work, the evolution of the liquid crystal is solved numerically using the lattice Boltzmann method [24–26]. Typical simulation parameters are shown in table I.

TABLE I: Simulation parameters

Symbol	Value	Units
A_0	0.5	atm
γ	3.103	—
K_1	10.72, 15	pN
K_2	10.72, 6.7	pN
K_3	10.72, 15	pN
Γ	0.33775	$atm^{-1}.\mu m^{-1}$
ξ	0.52	—
Δx	0.0625	μm
Δt	0.5	μs
P_0	1.0	atm

B. Colloid-Fluid interaction

The colloidal particles are spherical objects, and must be mapped onto the computational fluid mesh used by the lattice Boltzmann method. In order to couple the object to the fluid lattice, the object's surface must be discretized into a set of nodes (540 nodes were used for each colloid). An interpolation method is used to interpolate the nodes onto the fluid mesh to the nearest fluid lattice sites. Forces on the object, and the corresponding stresses in the fluid, can then be calculated. We outline this procedure below but the details of this method can be found in references [27–30, 47].

Objects moving through the liquid crystal experience forces from both the fact that fluid must move in order for the particle to move and also from the order parameter field of the liquid crystal due to the boundary conditions Eq. (5) and (6). Hydrodynamic forces are imposed by applying equal and opposite forces to corresponding sites on the fluid mesh and nodes representing the surface of the colloid:

$$\mathbf{F} = \pm\lambda(\mathbf{v}_n - \mathbf{u}_f), \tag{12}$$

where $\mathbf{v}_n$ is the particle node velocity and $\mathbf{u}_f$ is the velocity of the fluid interpolated to the particle node location. The plus sign corresponds to the local force acting on the fluid and the minus to the force on the colloid. The coefficient λ is chosen so that Eq. (12) leads to a good approximation to the no-slip boundary condition on the surface of the immersed particle, as detailed in [27, 28].

The effect of the colloid on the liquid crystal order is defined by the surface conditions, Eq. (5) and (6) and their corresponding term in the molecular field $\mathbf{H^{SC}}$ (Eq. (9)). These terms also contribute to the stress tensor and give rise to a contribution to the force on the surface of the colloid of the form

$$dF_\alpha = n_\beta \sigma^{SC}_{\alpha\beta} dS \tag{13}$$

where $\mathbf{n}$ is a unit normal pointing out, dS is a surface element of the colloid, and $\sigma^{SC}_{\alpha\beta}$ is the stress tensor Eq.(10) with just the contribution from the surface conditions, Eq. (5) and (6). Care must be taken to compute the force contribution from Eq.(13) only on the outside surface of the colloid [29], that the surface conditions contribution to the stress $\sigma^{SC}_{\alpha\beta}$ must also be excluded from the fluid stress to avoid double counting this force, and that Newton's third law is always satisfied[30, 47]. The colloid also experiences torques [30, 47], but these do not significantly impact the work done here as the colloids are spherical. The algorithm, including coupling forces, was implemented inside LAMMPS [48]. Further details of the numerical implementation, and its validation, can be found in [27–30, 47].

In the first part of the work, we fix the particles and just evolve the LC to steady state to map out the energy landscape. Later, we allow particles to move to find the locations of the energy minima. We will focus on shorter range interactions as these are the primary drivers of any self-assembled aggregates that might form.

III. RESULTS

In most of our simulations we consider two spherical colloidal particles with a radius of $0.625\mu m$ in a nematic liquid crystal inside a simulation box with dimensions of $L_x \times L_y \times L_z$. There are periodic boundary conditions imposed in the x and y directions, and fixed walls located at $z = 0$ and $z = L_z$, and the liquid crystal director has planar anchoring along a fixed direction on the walls, as shown in the figure 1. We use strong planar anchoring on the surface of one of the spherical particles, and normal anchoring on the other one. As a result, we have split core boojums at the poles of one sphere and a Saturn ring around the other one. The distances between the particles and the boundaries are large enough to minimize the effect of the boundaries on the particles, and the particles are initially placed in the $xy-$plane at $z = \frac{L_y}{2}$.

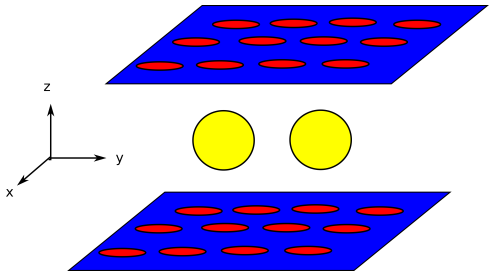

FIG. 1: Schematic of our system where the periodic boundary conditions are imposed in the x and y directions, the fixed walls are located in the z direction, and the liquid crystal molecules are set to be parallel on the walls (along $y-$axis for the nematic case and along the $x-$axis for the cholesteric).

A. Individual Spheres in a Nematic

Before considering two spheres, the well known defect structures of each of the individual spheres were investigated separately, for reference. Figure 2 shows the defect structure for planar and normal anchoring for isolated spheres in a nematic. In this figure, the pink lines correspond to defects, and show a contour plot of the positions around the particles where the scalar order parameter has decreased about 15% from the bulk value.

When we see inside the sphere, which in our simulations is a shell with LC both inside and out, there is an inner defect line which can be considered as the image of the outer defect lines in both cases. As the director field satisfies the linear Laplace's equation far from the colloidal particles, where deviations from uniformity are small [11, 21], it is analogous to electrostatics in which the electrostatic potential satisfies Laplace's equation as well. The surface of particle acts in a manner analogous to a conductor in electrostatics, and this analogy between the defect structures around the particles in a liquid crystal and charges in electrostatics was the motivation for the description in terms of dipole and quadrapoler far-field approximations. However, this analogy only holds for the far-field in nematics and does not work well for cholesterics, or close to the sphere and it is these near-field interactions that will control the local colloidal aggregates (ideally crystalline) that might form.

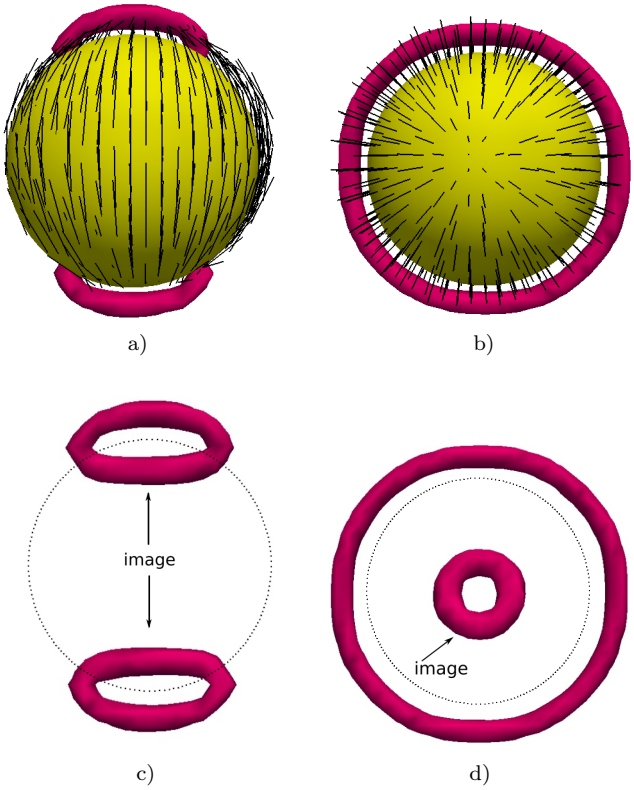

FIG. 2: The defects and their images for isolated particles in a nematic liquid crystal. In (a) and (c) the sphere has planar anchoring and in (b) and (d) the sphere has normal anchoring. The director is shown on the surface of the sphere in (a) and (b) and the sphere is not shown in (c) and (d), so that the image defects are visible.

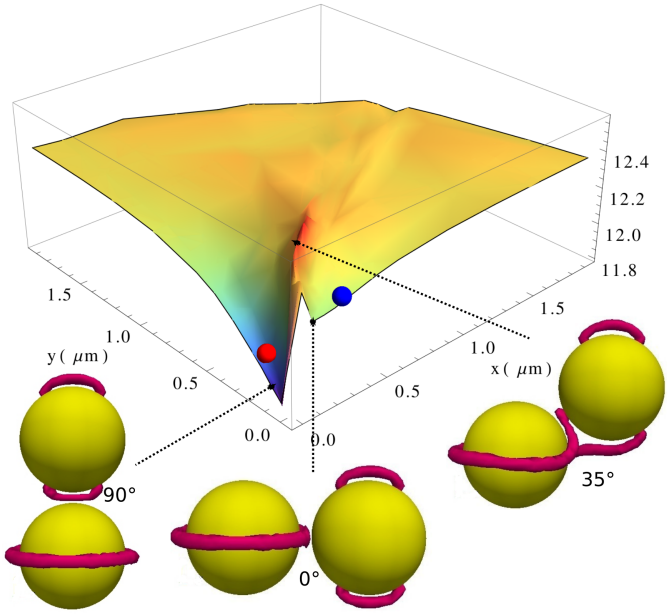

FIG. 3: Plot of the interaction energy surface for particles immersed in a nematic liquid crystal and confined to the $xy-$plane. Defect structures are shown for particles at a separation of $0.125\mu m$. The energy is measured at discrete separations on arcs with radii: 1/16, 1/8, 3/16, 1/4, 3/8, 1/2, 5/8, 15/16, 5/4, 3/2, 7/4, and 31/16 μm. The energies from the discrete points are then interpolated to produce the free energy surface. The blue and red points show the final relative position of freely moving particles when the initial positions have a separation of $0.25\mu m$ at the angles 0° and 35° respectively.

B. Interaction of Two Particles Immersed in a Nematic Liquid Crystal

Next, we consider these two particles placed together inside the nematic liquid crystal, where the director is parallel to the y-axis on the fixed walls. We investigate the possible defects when the particle with planar anchoring is rotated around the other one with normal anchoring, and located at different distances with respect to each other. In our work, all the angles are measured relative to the x axis. In this case, completely new defect configurations have been observed. As can be seen in figure 3, while the sphere is being rotated, the defect lines between the particles get connected to each other at about 35° and become disconnected at $\theta \geq 39°$. This kind of behavior can be seen up to a separation of about $0.375\mu m$ ($\sim \frac{1}{2}R$). The defect lines do not connect to each other at larger distances.

The interaction of these particles can be explored through a 3D contour of the interaction energy of system. As is shown in figure 3, the energy is maximized at $\theta \sim 35°$ and at a particle separation of $0.25\mu m$, where the defect lines are joined together, and there is a minimum at $\theta \sim 90°$ at small particle-particle separations.

There are several factors affecting the total energy of system. One is the length of the defect line. The presence of defect line inside the liquid crystal medium costs energy and as it gets longer, the total energy of system increases. Moreover, it is energetically favorable to have defect lines with strength of half integer instead of integral strength [21], since the energy of defect lines is proportional to the square of the defect strength. In addition to the length of defect lines, the energy of system can be decreased by reducing the volume of distortion in the director field, although the system may have to create a defect line to do so. There is also the surface energy of the director configuration on the particles surface. For the boojums (2a), this makes the two $m = \frac{1}{2}$ defects on the surface repel each other. The surface energy would be minimized by moving the defects as far apart as possible ($\sim 109°$ for tetrahedral symmetry [31]). The defects do not typically adopt this configuration as it would lengthen the defect line extending into bulk.

The maximum in energy at $\theta \sim 35°$ corresponds to the configuration where the defect lines get connected to each other resulting in them being longer at this angle, and since the defect lines cost energy, which is proportional to their length, the interaction energy is increased at this

angle. Presumably, failure to connect the defect lines at this point would create a much larger region of distortion which would cost even more energy. This is in contrast to the case examined by Mackay and Denniston in reference [32]. In that paper, the interactions of two particles, both with planar anchoring, was investigated inside a cholesteric liquid crystal. Since the length of the defect bond got shorter than a single defect bond in that case, it was energetically favorable for particle bonding to occur, which led to attraction. Also figure 4a and 4b, which plot the director field around the particles, shows that there is a slightly higher distorted volume around the particles at this angle than at the energy minimum. On the other hand, when the particles are close to each other at $\theta \sim 90°$, the plot of the director field indicates a very small region of distortion between the particles. As a result the particles are attracted to this position. There is also another local minimum at $\theta \sim 0°$ and at a distance of $0.125\mu m$.

Generally, the experimental results in reference [38] are consistent to our work as we found there are two local minima exist at $\theta = 0°$ and $\theta = 90°$ in the contour plot of interaction energy of colloids in nematic LC; however, the interaction energy for particles located along the director is lower as the energy is measured at smaller particle separations with smaller colloids.

C. Interaction of Particles Immersed in a Cholesteric Liquid Crystal in the $xy-$Plane

We now switch the medium from nematic to cholesteric liquid crystal. As the properties of a cholesteric liquid crystal can be dependent on the value of its pitch, several pitch values have been examined to measure the interaction energy. The values that were selected, 1.5 μm, 3 μm, and 1.125 μm, are close to the size of the particle, larger, and smaller than the particle size, respectively. The system size in the $z-$direction is always an integer or $1/2$ integer multiple of the pitch so that the fixed anchoring along the walls, along the $x-$axis here, corresponds to a relaxed state in the absence of the colloids.

Again two spheres with binary applied boundary conditions, i.e. one planar and one normal are put inside the cholesteric, starting with the pitch value of 1.5 μm, and the particle with planar anchoring is rotated around the other sphere while they are separated at a variety of distances. In this case, completely different defect structures were observed from those seen in the nematic. Since the medium is cholesteric, the defect lines are twisted around the particles [17]. As can be seen in figure 5a, when the particles are separated $0.125\mu m$ from each other, the boojum defect lines and the Saturn ring are joined together from both sides of the particles. While the particle is being rotated around the other one, the Saturn ring gets connected to the surface of the other particle in the middle, at $\theta \sim 25°$. This kind of structure is observed up to $\theta \sim 55°$. At this configuration, there is

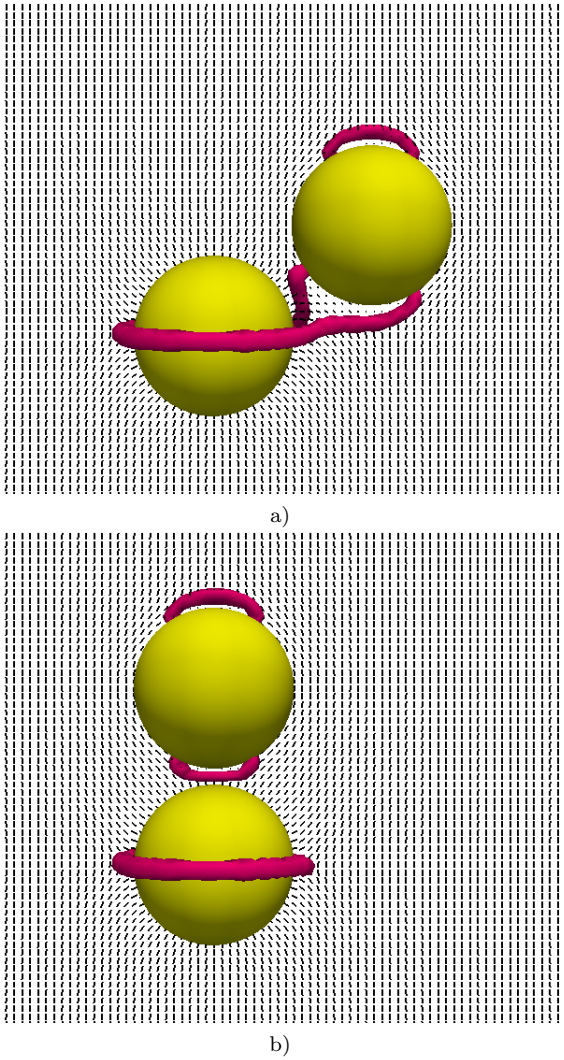

a)

b)

FIG. 4: Plot of the director field around the particles inside a nematic LC and located on the $xy-$plane with separation of a) $0.25\mu m$ at $\theta = 35°$, and b) $0.125\mu m$ at $\theta = 90°$.

a point where the defect lines of both particles are joined together. At $\theta \sim 60°$, the defect lines are only connected on one side. The most fascinating defect structure happens at $\theta \sim 85°$. At this position, the defect lines are connected not only on both sides, but also at two points in the middle of the particles, which looks like a symmetric defect structure. At $\theta \sim 90°$, this symmetric defect is not seen.

The same sorts of defect structure can be seen at different angles at a separation of $0.25\mu m$. When the particles are separated $0.375\mu m$ from each other, no defect lines are connected between the particles up to $\theta \sim 43°$, which is shown in figure 5a. At $\theta \sim 43°$ the defect lines are connected at two points at one side of the particles. At $\theta \geq 55°$, the lines are not joined at any points but there is a connection of defect lines at one side and in between the spheres. Furthermore, at $\theta \sim 90°$, there is one point where the defects are connected as well. At a separa-

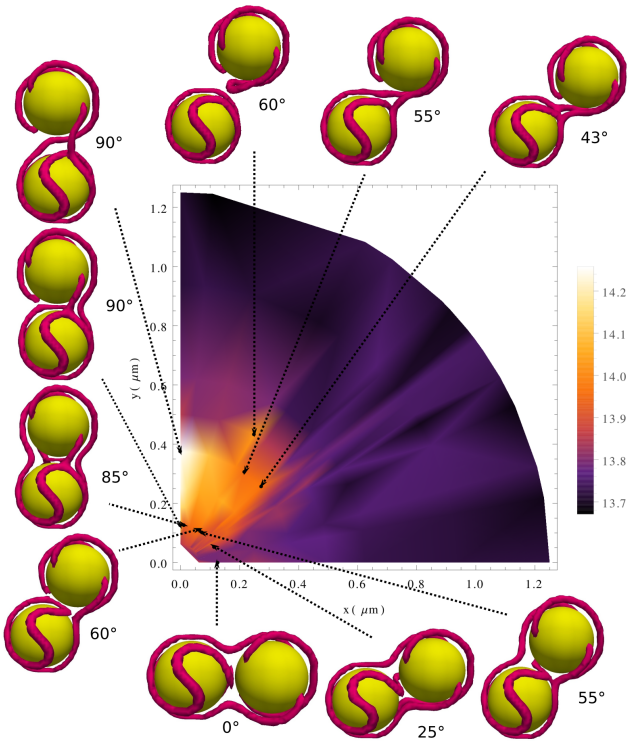

a)

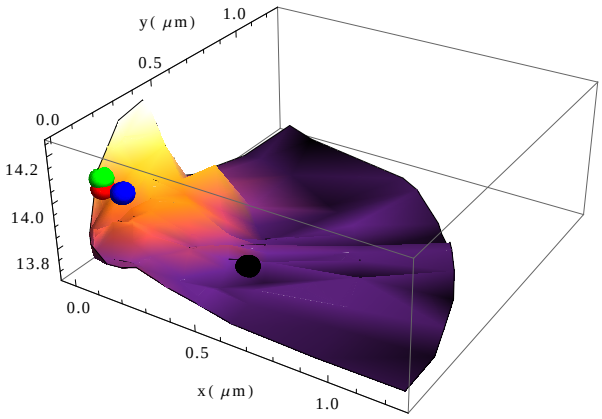

b)

FIG. 5: a) 2D plot of interaction energy for the particles immersed in the cholesteric liquid crystal in the $xy-$plane with pitch value of $1.5\mu m$ along with some corresponding defect structures and b) a 3D plot of the interaction energy. The energy is measured when the particles are located at several points on arcs with radii: $0.0625\mu m$, $0.125\mu m$, $0.1875\mu m$, $0.25\mu m$, $0.375\mu m$, $0.5\mu m$, $0.625\mu m$, $0.9375\mu m$, $1.25\mu m$. The energies from the discrete points are then interpolated to produce the free energy surface. The red, blue, black and green points are the final relative position of freely moving particles when the initial positions are: separation $0.125\mu m$ at $90°$, $0.25\mu m$ at $55°$, $0.375\mu m$ at $25°$, and $0.375\mu m$ at $90°$.

tion of $0.5\mu m$, no connection occurs, while the boojum defect lines become different in shape at $\theta \sim 60°$, as is exhibited in figure 5a. At larger separations, no defect lines are joined together. In the plot of the interaction energy of particles, figures 5a and 5b, there is a sharp maximum in energy at $\theta \sim 90°$, where the particles are separated about $0.375\mu m$ from each other and the defect lines are joined at one common point at one side and there is a defect line connected to other sphere which is passed in between the particles. It seems that the defect lines get more stretched at this specific configuration, so it can be concluded that the total length of defect lines is higher than other positions, which leads to increase in the energy. So there is a repulsion when the particles approach each other from far distances, but attraction at short distances.

Next, the defect structures and interaction of two particles is investigated in a cholesteric with the lower pitch value of $1.125\mu m$, which is smaller than the particle diameter. In this case, the defect lines are much more twisted around the particles. Figure 6a shows the 2D plot of interaction energy as well as the defect structures of particles at different angles and separations.

When the particles are kept at a separation of $0.125\mu m$, two twisted defect lines join together from both sides and a defect in the shape of a handle appears on the surface of the particle with planar anchoring at $\theta \sim 0°$. At $\theta = 25°$, the Saturn ring starts to join to the handle defect, so the defect in between the particles does not look like a handle any more. This kind of structure can be seen up to $\theta \sim 45°$. At this angle, there is a point on one side of the particles where the defect lines are joined together. This kind of defect can be observed up to $\theta \sim 85°$. At $\geq 85°$, the defect lines are only connected around the particles. Then the particle separation is increased to $0.1875\mu m$. As seen in figure 6a, one of the twisted defect lines cycles around the particles at this point. This structure is seen up to $\theta \sim 15°$. At this angle, again the defect lines are joined at a point on one side of the particles; however, the Saturn ring is only connected to the other particle at $\theta \sim 25°$ in between the particles, and the same structure remains for larger angles. At $\theta \geq 55°$, there is a point where three defect lines are joined on one side and we can see a symmetric defect structure in between the particle at $\theta = 90°$. The same sort of defects are seen at higher separations but at different angles. There is no connection in defect lines for larger distances than $0.25\mu m$.

If we look at the plots of the energy of the particles, as shown in figure 6a and 6b, we see that the interaction energy peaks at $\theta \sim 55°$ at a particle separation of about $0.25\mu m$. At this point the defect lines are connected between the particles and the total length of lines appears to be higher, accompanied by an increase the distortion volume. The energy is minimized at $\theta \sim 0°$ when they are very close to each other, $\sim 0.0625\mu m$. Figure 7a and 7b shows a cross-section of the elastic energy of the system at the extrema. One can see that there is a much larger

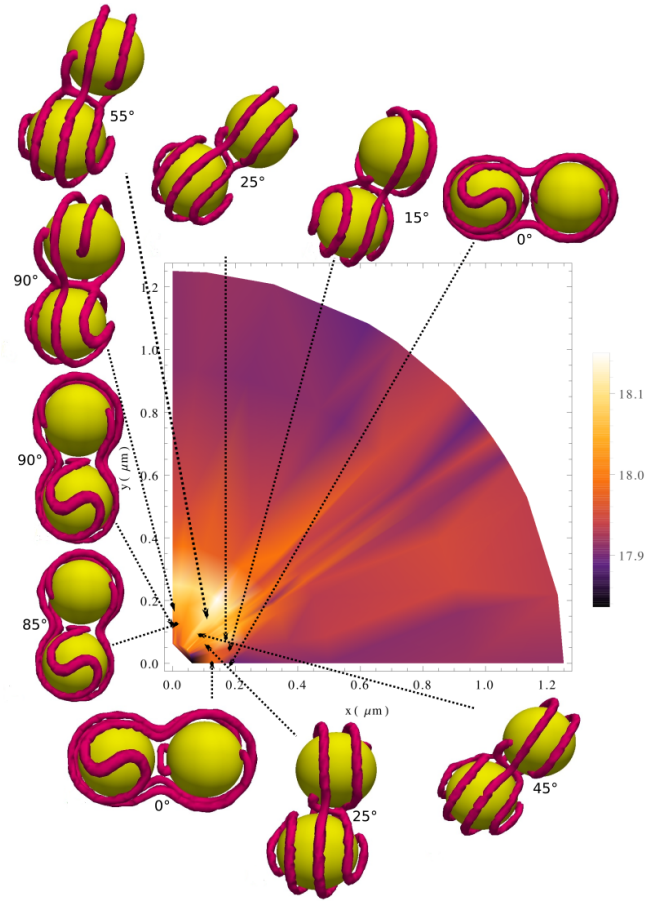

a)

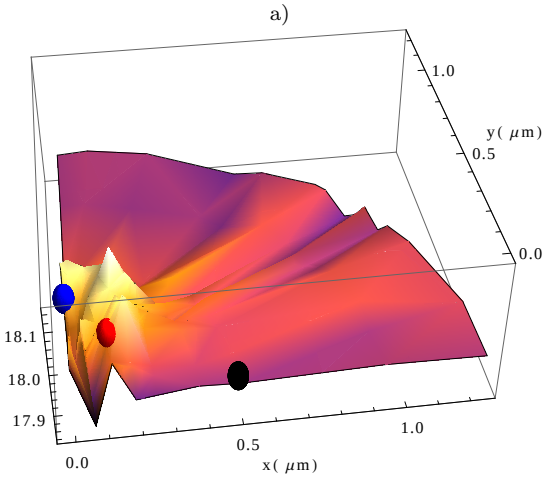

b)

FIG. 6: a) 2D plot of interaction energy for the particles immersed in the cholesteric liquid crystal in the $xy-$plane with pitch value of $1.125\mu m$ with their defect structures and b) a 3D plot of the interaction energy. The energy is measured when the particles are located at several points on arcs with radii: $0.0625\mu m$, $0.125\mu m$, $0.1875\mu m$, $0.25\mu m$, $0.375\mu m$, $0.5\mu m$, $0.9375\mu m$, $1.25\mu m$. The energies from the discrete points are then interpolated to produce the free energy surface. The blue, red, and black points correspond to the final relative position of freely moving particles when the initial positions are: separation $0.375\mu m$ at $90°$, $0.25\mu m$ at $55°$, and $0.375\mu m$ at $0°$.

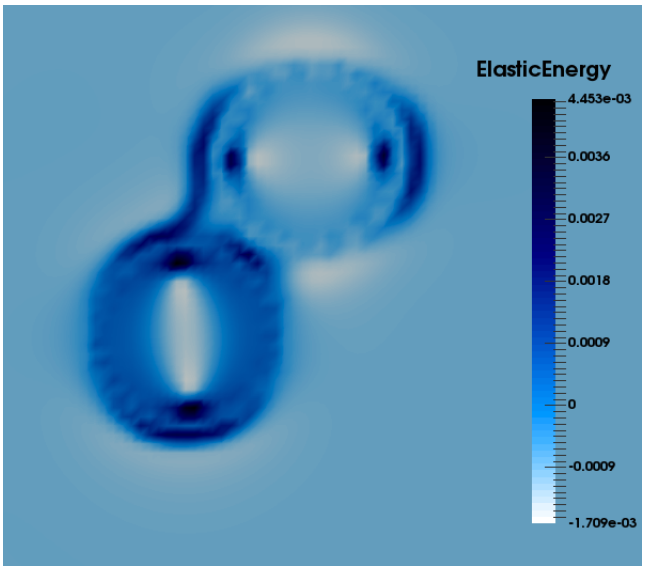

a)

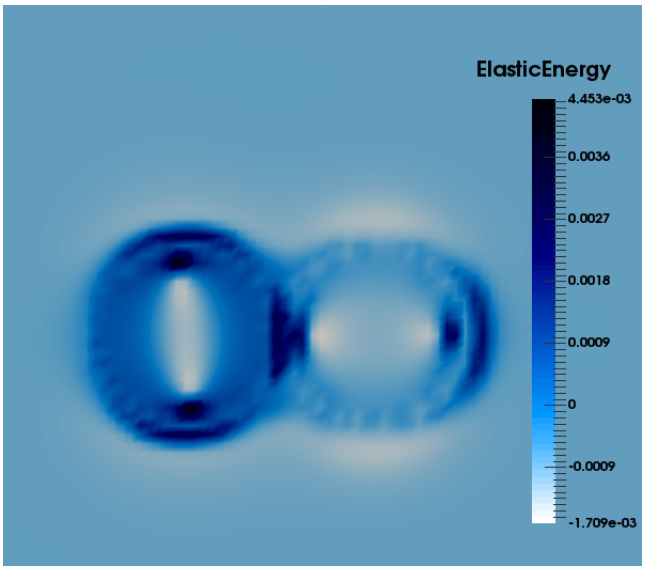

b)

FIG. 7: a) 2D plot of elastic energy for the particles immersed in the cholesteric liquid crystal in the $xy-$ plane with pitch value of $1.125\mu m$ at a) particle separation of $0.25\mu m$ and the angle $55°$, and b) separation of $0.0625\mu m$ at the angle $0°$.

overlap in the distortion in Fig.7b (the minimum)than in Fig. 7a (the maximum). Looking at the bigger picture in Fig.6a and 6b we see that the interaction is primarily repulsive at larger distances and only becomes attractive at close separations and not at all angles.

Finally, we increase the value of the pitch to 3 μm and see the defect lines are less twisted around the particles (Fig.8). When the particles are separated $0.125\mu m$, it is observed in figure 8 that the defect lines of particles start to get connected at $\theta \sim 15° - 25°$, and disconnected for $\theta \geq 60°$. The same sort of structure is observed up to a particle separation of $0.375\mu m$. Comparing Fig. 8 and Fig. 3, we see that the interaction energies and topology

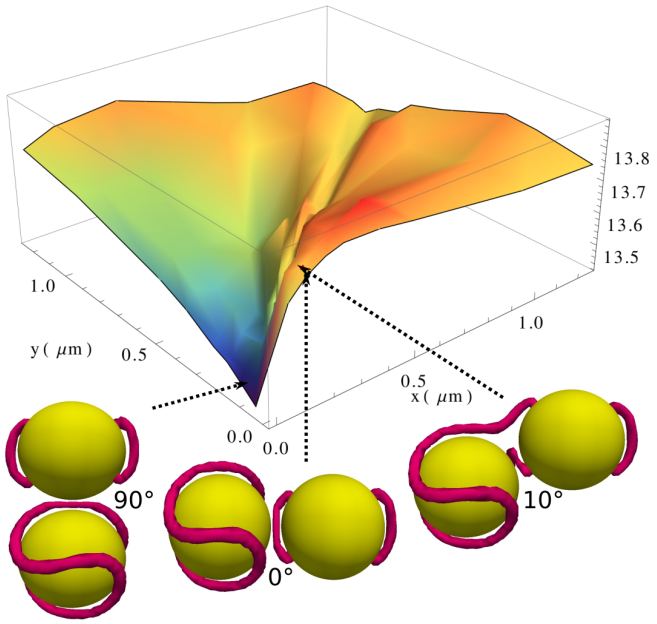

FIG. 8: 3D plot of interaction energy when the cholesteric pitch is 3 μm. The energy is measured when the particles are located at several points on arcs with radii: $0.0625\mu m$, $0.125\mu m$, $0.1875\mu m$, $0.25\mu m$, $0.375\mu m$, $0.5\mu m$, $0.9375\mu m$, $1.25\mu m$.

of the defect structures in the cholesteric liquid crystal with pitch larger than the particle diameter are quite similar to the nematic case. As can be seen in figure 8, the interaction energy is maximized at about 10°, at a separation of $0.375\mu m$. Also there is a minimum in energy when the particles are very close to each other at $\theta \sim 90°$. The repulsion and attraction between the particles can be further illuminated through the plot of a cross-section of the elastic energy which is shown in figure 9. There is more overlap in the region of high elastic energy (higher distortion) at the minimum (Fig. 9(b)) than at the maximum (Fig. 9(a)).

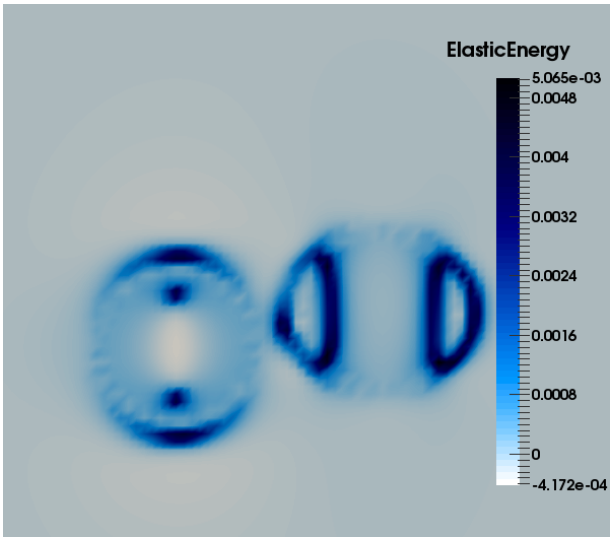

a)

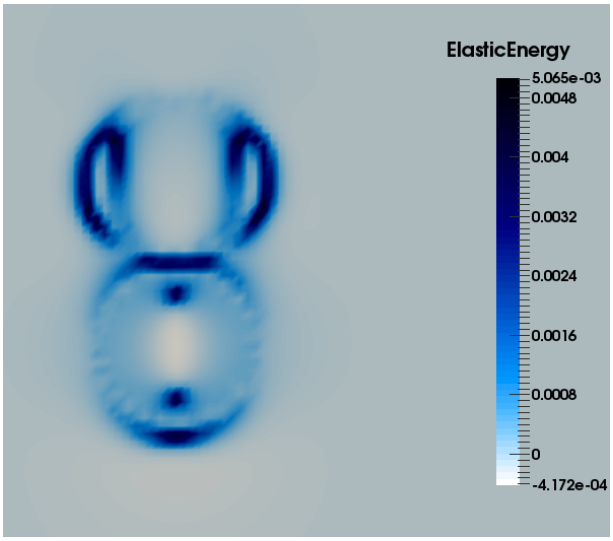

b)

FIG. 9: a) 2D plot of elastic energy for the particles immersed in the cholesteric liquid crystal in the $xy-$ plane with pitch value of $3\mu m$ at a) particle separation of $0.375\mu m$ and the angle 10°, and b) separation of $0.0625\mu m$ at the angle 0°.

D. Interactions of Particles Immersed in the $xz-$Plane

So far the spheres have been confined to the $xy-$plane where the minima for homogeneous particles [17] were found. Exploring all of space is too computationally expensive, but one step in this direction is investigating the possible induced interactions between the particles, and the induced defect structures, when they are rotated within the $xz-$plane and the spheres are fixed at $y = \frac{L_y}{2}$.

First, the particles are put in the nematic, and again the particle with planar anchoring is rotated around the other particle, separated at different distances. Figure 10 shows the configuration of particles in which they are kept at a distance of $0.125\mu m$ with respect to each other. Unlike the spheres confined to the $xy-$plane, the defect lines no longer connect to each other. Examining to the contour plot of interaction energy in figure 10, we see the energy is lower when they are close to each other (up to a separation of about $0.5\mu m$) and does not vary much with the angle. The energy increases as they are pulled apart from each other, meaning they are attracted to small separations. This can be justified by focusing at the plot of director field around the particles which is illustrated in figure 11. As seen in the figure, when the particles are close to each other, there is only a very small region around the particles where the director field becomes distorted from its uniform orientation. On the other hand, if they are farther apart there is a larger region between them of director distortion leading to an

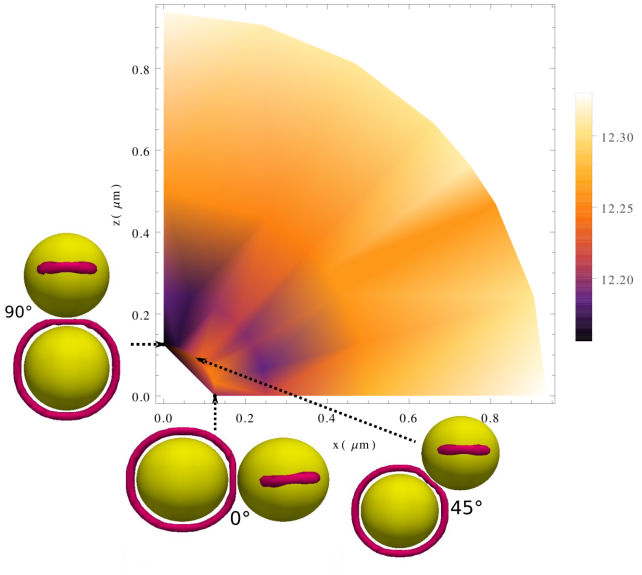

FIG. 10: 2D contour plot of interaction energy of 2 particles in a nematic in the $xz-$plane along with some corresponding defect structures. The energy is measured when the particles are located at several points on arcs with radii: $0.0625\mu m, 0.125\mu m, 0.25\mu m, 0.5\mu m, 0.9375\mu m$.

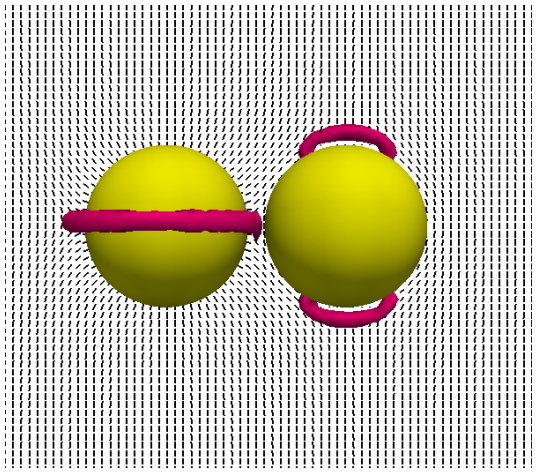

a)

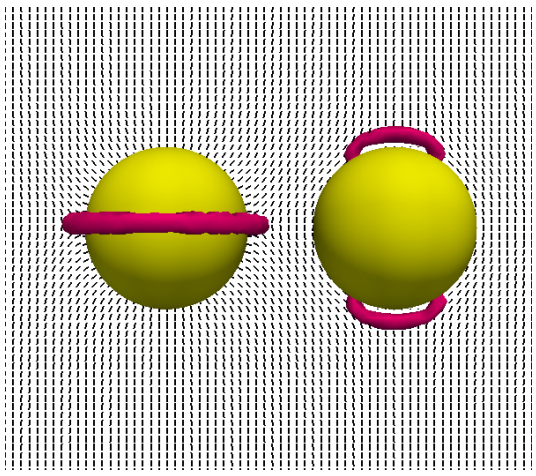

b)

FIG. 11: Plot of director field of particles in the $xz-$plane for the particle separations of a)$0.125\mu m$ and b)$0.5\mu m$ when $\theta = 0°$. The colloids/defects are viewed along the $z-$axis.

increase in the interaction energy.

We can now compare the results obtained for both $xy-$ and $xz-$planes. If we compare the particles placed on the $xy-$plane versus the $xz-$plane, we notice that the lowest minimum in energy occurs on the $xy-$plane rather than the $xz-$ plane. Therefore, it can be concluded that the minimum in energy is likely to be in $xy-$plane for particles inside a nematic liquid crystal. The result is that groups of larger numbers of such particles are likely to form either chains or planar structures, similar to what is seen for particles with all planar anchoring in nematic and cholesteric liquid crystals [24, 33].

Next, the particles are placed into a cholesteric with a pitch of $1.5\mu m$. We focus on this pitch as it was the most interesting case from our examination of interactions in the $xy-$plane. Figure 12 shows the defect structures of the two particles as well as a 2D plot of their interaction energy. When the particles are at a distance of $0.25\mu m$, we see that the boojums and the Saturn ring are joined together between the particles at $\theta = 0°$. At $\theta = 15°$, the defect lines are joined into one defect line, which is surrounding around the particles. The similar kind of defect structure is seen at $\theta = 45°$; however, the boojums are only connected to the ring at the pole of the particle with normal anchoring at $\theta = 60°$. No defect lines are joined together for angles greater than 75°. For particle separations of 0.5 μm and greater the defect lines do not connect. As can be seen in figure 12, the energy is maximized at $\theta \sim 15°$ near a particle separation of $0.25\mu m$, while it is minimized at $\theta \sim 60°$ again near a separation of $0.25\mu m$. In fact, this minimum appears to be slightly lower than any found in the $xy-$plane (fig. 5a) suggesting the global minimum is not in the $xy-$plane, unlike the previous cases. In addition, the minimum in the $xz-$plane is within a deeper "canyon" structure compared to the surrounding energy landscape compared to the minimum found in the $xy-$plane. It seems possible that in this case there are multiple nearly degenerate minima, perhaps not all in a coordinate plane.

The case with particles in the cholesteric with a pitch of $3\mu m$ was similar to the nematic case in the $xy-$plane and we expect similar results in the $xz-$plane so we did not further investigate that case here. Similarly, the case with the tighter pitch, $1.125\mu m$ was somewhat similar to the intermediate pitch case so we did not investigate it further in the $xz-$plane.

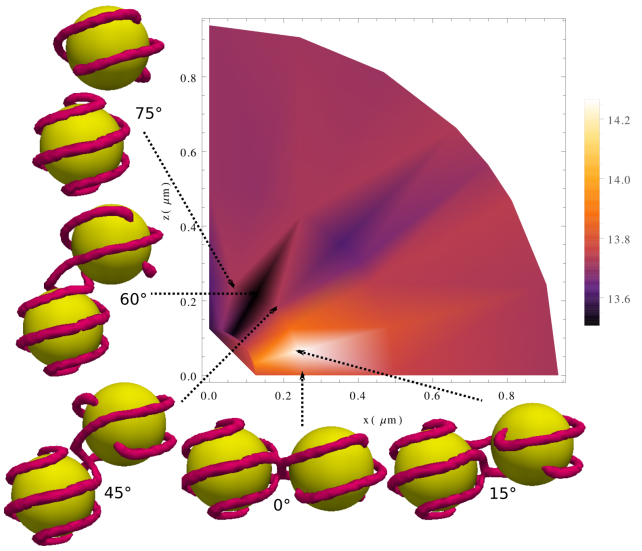

FIG. 12: 2D contour plot of interaction energy of 2 particles in the $xz-$plane with the defect structures in a cholesteric LC with a pitch of $1.5\mu m$. The energy is measured when the particles are located at several points on arcs with radii: $0.0625\mu m, 0.125\mu m, 0.25\mu m, 0.5\mu m, 0.9375\mu m$.

E. Freely Moving Particles

So far, we have investigated only static particles inside the LC, confined to either the $xy-$ or $xz-$planes. It is, of course, possible that the particles experience local minima in other positions. Therefore, we performed the simulations where particles are free to move in the medium to see what positions they are attracted to, and if their movements are consistent with what we observed in the static simulations. In this section, the particles are free to move based on the forces they experience from the liquid crystal stress tensor. At very close range the colloids should experience a hard sphere repulsion which would prevent overlaps. We implement this as a short-range Lennard-Jones interaction cutoff at it's minimum so that it is purely repulsive.

$$V(r) = \begin{cases} 4\epsilon\left[\left(\frac{\sigma}{r}\right)^{12} - \left(\frac{\sigma}{r}\right)^{6}\right] - \epsilon, & \text{if } r \leq r_c \\ 0, & \text{if } r > r_c, \end{cases} \tag{14}$$

where $\sigma = r_c/2^{1/6}$ and $r_c = 0.125\mu m$. ϵ was set to $2.5\times10^{-8} atm/\mu m$ so the behavior is primarily dominated by liquid crystal forces until the particles nearly touch.

1. *Nematic LC*

We chose several different initial positions for the particles on the $xy-$plane inside the nematic LC. When the particles are initially separated $0.25\mu m$ from each other at $\theta = 0°$ (i.e. near the local energy minimum), there is not much change in their position as a function of time; however, when the particles are initially separated $0.25\mu m$ from each other at $\theta = 35°$, the particle with planar anchoring rotates toward the pole of the other particle, corresponding to the positions inside the LC where the interaction energy is lower as seen in figure 3. The final positions of the particles are indicated on figure 3. Also, particles initially placed further apart get closer to each other, consistent with the previously measured free energy surface. In all cases, the particles remain on the $xy-$plane, and go to one of the minima seen in figure 3.

2. *Cholesteric LC*

Similar simulations were carried out for particles in the cholesteric LC with pitches of $1.5\mu m$ and $1.125\mu m$. When the particles in the cholesteric LC with a pitch of $1.5\mu m$, are started at a separation of $0.125\mu m$, and $\theta = 90°$, it is observed that their relative distance and orientation do not vary very much. This is consistent with figure 5, showing the energy increases when the particle separation increased to $0.375\mu m$ at the same orientation, so this appears to be a local minimum. The particles were also initially placed at a distance of $0.25\mu m$ at $\theta = 55°$. In this case, the particles get slightly closer and their relative angle with respect to $x-$axis does not change very much. Furthermore, the particles' relative distance increases to $0.5625\mu m$ and the orientation do not undergo a dramatic change, when they are initially separated at $0.375\mu m$ at $\theta = 25°$. Both these locations are local minima in Figure 5. On the other hand, when the particles are located at the place where the energy is maximized (separation of $0.375\mu m$ and $\theta = 90°$), particles get closer to each other, toward the nearby minimum, even though it may be expected that the particles get farther from each other where the energy decreases faster. The reason is probably related to the local defect configuration being closer to that of the nearby minimum rather than the one along the direction of what appears to be the steepest descent. One should keep in mind that the surface plotted in the figure represents the lowest energy state found for particles with this separation (the initial configurations used in the plot were defect free and so the defects formed spontaneously *at that separation* and so were more likely to find the minimum for that given separation). It is quite possible to find particles at the same separation with higher energy due to a different defect configuration. Hence the barriers for moving from one state to another may be higher than expected from the plot.

In general, for both pitches, we found that if we started particles near a local minimum, they typically found it. However, if particles were started far from a local minimum they usually found the minimum but sometimes did not and instead got stuck in a higher energy state. Examination of these stuck configurations showed that they would have had to break and reconfigure a defect line to get to the minimum. Clearly in those cases the

barrier to doing this was too high. In no cases did the particles find a configuration with lower energy than the free energy surface plotted in the figures (i.e. this surface does seem to be a lower bound for the free energy) .

IV. CONCLUSION AND DISCUSSION

In this work, we studied the interaction of two colloidal particles with different anchoring, planar and normal, in both a nematic and cholesteric LC.

In the nematic, there is a quite prominent minimum of the free energy for separations in the $xy-$plane along a fixed direction (90deg in Fig. 3). There is also a local minimum at 0 deg as well. The free energy for separations in the $xz-$plane was higher, much more uniform, with nearly radial symmetry. This would suggest that mixtures with larger numbers of pairs are likely to form linear chain configurations, similar to what is seen for particles all with the same anchoring condition in a nematic [15, 34].

When the medium is changed to a cholesteric, the result depends on the pitch. In systems with pitch larger than the particle size, the defect structure seen is topologically similar to that seen in the nematic case, with the main difference being somewhat more winding of the saturn-ring defect. The free energy structure is also similar, again suggesting that mixtures with more than one pair are likely to form linear chains.

When the cholesteric pitch is comparable to, or smaller than, the particle size the defect lines are much more likely to get attached to each other and produce a new set of structures due to the high twist of the lines. The results are different from the defect-bonded chains produced by particles where both had planar achoring in a cholesteric LC in [17]. In this case there are multiple local minima, and not all in the same plane. In addition, the interaction changes from attractive to repulsive at quite short ranges. Together, this suggests that large number of these pairs may form fairly complex binary crystal structures, and not necessarily close-packed ones. Therefore, we are left with some open questions that must be considered as our future work. There are probably some unexplored global minima existing in the 3D space that are not located in the plane. Considering these kinds of minima, we can investigate what type of stable colloidal crystals can be produced as our future work. Furthermore, the size of pitch affects the existence of minima in free energy. We must look for the lowest energy crystals made of up colloids with binary surface anchoring in cholesteric LC and tune the size of pitch producing the ideal colloidal crystals

Acknowledgments

We would like to thank the Natural Science and Engineering Research Council of Canada (NSERC) for financial support. This research has been enabled by the use of computing resources provided by Shared Hierarchical Academic Research Computing Network (SHARCNET) and Compute/Calcul Canada.

[1] H. Cong, B. Yu, J. Tang, Z. Li, and X. Liu, Chem. Soc. Rev. **42**, 7774 (2013), URL `http://dx.doi.org/10.1039/C3CS60078E`.
[2] Y. Xia, B. Gates, and Z.-Y. Li, Advanced Materials **13**, 409 (2001), ISSN 1521-4095.
[3] J. Ge and Y. Yin, Angewandte Chemie International Edition **50**, 1492 (2011), ISSN 1521-3773.
[4] M. Skorobogatiy and J. Yang, *Fundamentals of Photonic Crystal Guiding* (Cambridge University Press, 2009).
[5] J. Joannopoulos, S. Johnson, J. Winn, and R. Meade, *Photonic Crystals: Molding the Flow of Light, 2nd ed.* (Princeton University Press, 2008).
[6] A. Massaro, *Photonic Crystals - Introduction, Applications and Theory* (InTech, 2012).
[7] P. Poulin and D. A. Weitz, Phys. Rev. E **57**, 626 (1998).
[8] H. Stark, Physics Reports **351**, 387 (2001), ISSN 0370-1573.
[9] M. Tasinkevych, N. M. Silvestre, and M. M. T. da Gama, New Journal of Physics **14**, 073030 (2012).
[10] M. Kleman and O. D. Lavrentovich, Philosophical Magazine **86**, 4117 (2006).
[11] T. C. Lubensky, D. Pettey, N. Currier, and H. Stark, Phys. Rev. E **57**, 610 (1998).
[12] Y. Gu and N. L. Abbott, Phys. Rev. Lett. **85**, 4719 (2000).
[13] O. V. Kuksenok, R. W. Ruhwandl, S. V. Shiyanovskii, and E. M. Terentjev, Phys. Rev. E **54**, 5198 (1996).
[14] O. Guzmán, E. B. Kim, S. Grollau, N. L. Abbott, and J. J. de Pablo, Phys. Rev. Lett. **91**, 235507 (2003).
[15] I. I. Smalyukh, O. D. Lavrentovich, A. N. Kuzmin, A. V. Kachynski, and P. N. Prasad, Phys. Rev. Lett. **95**, 157801 (2005).
[16] J. S. Lintuvuori, D. Marenduzzo, K. Stratford, and M. E. Cates, J. Mater. Chem. **20**, 10547 (2010).
[17] F. E. Mackay and C. Denniston, EPL (Europhysics Letters) **94**, 66003 (2011).
[18] T. C. Lubensky, D. Pettey, N. Currier, and H. Stark, Phys. Rev. E **57**, 610 (1998).
[19] I. Musevic, M. Skarabot, U. Tkalec, M. Ravnik, and S. Zumer, Science **313**, 954 (2006), ISSN 00368075, 10959203, URL `http://www.jstor.org/stable/3846976`.
[20] F. E. Mackay and C. Denniston, Soft Matter **10**, 4430 (2014).
[21] P. G. de Gennes and J. Prost, *The Physics of Liquid Crystals* (Oxford University Press, 1993).
[22] A. N. Beris and B. J. Edwards, *Thermodynamics of Flowing Systems: with Internal Microstructure* (Oxford Engineering Science Series, 1994).
[23] J.-B. Fournier and P. Galatola, EPL (Europhysics Let-

ters) **72**, 403 (2005).
[24] C. Denniston, D. Marenduzzo, E. Orlandini, and J. M. Yeomans, Philosophical Transactions of the Royal Society of London A: Mathematical, Physical and Engineering Sciences **362**, 1745 (2004), URL http://rsta.royalsocietypublishing.org/content/362/1821/1745.
[25] C. Denniston, E. Orlandini, and J. M. Yeomans, Phys. Rev. E **63**, 056702 (2001), URL http://link.aps.org/doi/10.1103/PhysRevE.63.056702.
[26] C. Denniston, E. Orlandini, and J. M. Yeomans, EPL (Europhysics Letters) **52**, 481 (2000), URL http://stacks.iop.org/0295-5075/52/i=4/a=481.
[27] F. Mackay, S. Ollila, and C. Denniston, Computer Physics Communications **184**, 2021 (2013), ISSN 0010-4655.
[28] F. Mackay and C. Denniston, Journal of Computational Physics **237**, 289 (2013), ISSN 0021-9991.
[29] F. E. Mackay and C. Denniston, Soft Matter **9**, 5285 (2013).
[30] A. Antipova and C. Denniston, Soft Matter **12**, 1279 (2016).
[31] D. R. Nelson, Nano Letters **2**, 1125 (2002).
[32] F. E. Mackay and C. Denniston, EPL (Europhysics Letters) **94**, 66003 (2011).
[33] N. Hijnen, T. A. Wood, D. Wilson, and P. S. Clegg, Langmuir **26**, 13502 (2010), pMID: 20695597, http://dx.doi.org/10.1021/la101420c.
[34] M. R. Mozaffari, M. Babadi, J.-i. Fukuda, and M. R. Ejtehadi, Soft Matter **7**, 1107 (2011).
[35] M. Ravnik, G. P. Alexander, J. M. Yeomans, S. Žumer, and N. A. Clark, Proceedings of the National Academy of Sciences of the United States of America **108**, 5188-5192 (2011).
[36] T. A. Wood, J. S. Lintuvuori, A. B. Schofield, D. Marenduzzo, and W. C. K.Poon, Science **334**, 79–83 (2011).
[37] K. Stratford, O. Henrich, J. S. Lintuvuori, M. E. Cates, and D. Marenduzzo, NATURE COMMUNICATIONS **5**, 3954 (2014).
[38] U. M. Ognysta, A. B. Nych, V. A. Uzunova, V. M. Pergamenschik, V. G. Nazarenko, M. Škarabot, and I. Muševič, Phys. Rev. E **83**, 041709 (2011).
[39] V. S. R. Jampani, M. Škarabot, S. Čopar, S. Žumer, and I. Muševič, Phys. Rev. Lett. **110**, 177801 (2013).
[40] J. S. Lintuvuori, K. Stratford, M. E. Cates, and D. Marenduzzo, Phys. Rev. Lett. **107**, 267802 (2011).
[41] R. P. Trivedi, M. Tasinkevych, and I. I. Smalyukh, Phys. Rev. E **94**, 062703 (2016).
[42] D. F. Gardner, J. S. Evans, and I. I. Smalyukh, Molecular Crystals and Liquid Crystals **545**, 3/[1227]-21/[1245] (2011).
[43] I. Musevic,and M. Skarabot Soft Matter **4**, 195-199 (2008).
[44] I. Muševič Liquid Crystals **36**, 639-647 (2009).
[45] I. Muševič Liquid Crystals Today **19**, 2-12 (2010).
[46] N. Hijnen, T.A. Wood, D. Wilson, and P.S. Clegg, Langmuir **26**, 13502 (2010).
[47] A. Antipova and C. Denniston, Phys. Rev. E **94**, 052704 (2016).
[48] S. Plimpton, J. Comput. Phys. **117, 1 (1995).**